Volume 10, Issue 1, 2020, 4956 - 4965 ISSN 2069-5837
Biointerface Research in Applied Chemistry
www.BiointerfaceResearch.com
https://doi.org/10.33263/BRIAC101.956965
Original Research Article Open Access Journal
Received: 29.11.2019 / Revised: 18.01.2020 / Accepted: 20.01.2020 / Published on-line: 23.01.2020

Bio-capacitor consist of insulated myelin-sheath and uninsulated node of Ranvier: a bio-nano-antenna

Majid Monajjemi [1], Fatemeh Mollaamin [2]
Department of chemical engineering, Central Tehran Branch, Islamic Azad University, Tehran, Iran
*corresponding author e-mail address: ***maj.monajjemi@iauctb.ac.ir*** | Scopus ID 6701810683

ABSTRACT
Myelin consists of fatty molecules (lipids) which are located in the CNC (central nervous system) and as an insulator around nerve cell axons increases the velocities information to transit from one nerve cell to another tissue like an electrical wire (the axon) with insulating material (myelin) around it. Each axon contains multiple long myelinated parts separated from each other through short gaps called "Nodes of Ranvier" or myelin-sheath gaps. A computational model is presented for the simulation of propagated electromagnetic waves in a critical point between insulated myelin-sheath towards uninsulated node of Ranvier. The QM/MM calculation has been applied for generalizing the node of Ranvier results for computing action potentials and electro chemical behavior of membranes which agree with clusters of voltage-gated ion sodium and potassium channels. The node of Ranvier complexes is an accurate organization of membrane-bound aqueous compartments, and the model presented here represents electrophysiological events with combined realistic structural and physiological data. The quantum effects of different thicknesses in the mixed membranes of GalC/DPPC, have also been specifically investigated. It is shown that quantum effects can appear in a small region of free spaces within the membrane thickness due to the number and type of lipid's layers. In addition, from the view point of quantum effects by Heisenberg rule, it is shown that quantum tunneling is allowed in some micro positions of membrane capacitor systems, while it is forbidden in other forms.
Keywords: *lipid bilayers; variable capacitors; cell membrane capacitors; node of Ranvier; myelin-sheath.*

1. INTRODUCTION
A Node of Ranvier (NOR) is uninsulated and fully enriched in ion channels, permitting them to interfere in the ion exchanging to produce sufficient action potentials. Nerves conduction in the myelinated axons is a kind of jumping due to the high action potential from one node to the next node [1-3]. In other words, reducing axonal membrane capacitance through insulating the axon increases the action potential due to large distances between the cations on the outside of the axon and Na^+ that move through the axonal cytoplasm (axoplasm) [4]. Since the length neither of NOR (around one micron) compares to adjacent long myelinated internodes (around one millimeter) is too much shorter (1000 times), suddenly an electrical signal in a critical point between insulated myelinated towards uninsulated of unmyelinated stimulates the release of a chemical message or neurotransmitter that binds to receptors on the adjacent post-synaptic cell at specified area called synapses [5, 6]. The insulating structure for myelin is important for hearing, seeing, feeling, sensation of pain and as well as perception, knowledge and memory. Therefore, multiple sclerosis which specifically affects the central nervous system, is related to disordering of myelin [7, 8]. The major operation of myelin is providing acceleration to electrical impulses propagate along the myelinated fiber [9]. Although in unmyelinated fibers, electrical impulses move as continuous waves, in myelinated fibers they are propagated via saltatory conduction which is faster than continues wave [1]. Myelin reduces the capacitor capacitance consequently enhances the electrical resistance across the axonal membrane [10]. Voltage-gated sodium channels are highly abundant at the nodes of Ranvier, Na^+ can enter the axon via these voltage-gated channels, leading to depolarization of the membrane potential at the node of Ranvier [11]. The resting membrane potential is then quickly repaired due to K^+ ions leaving the axon through potassium channels. The Na+ inside the axon quickly diffuses via the axoplasm to the inter-node and then to the next node of Ranvier for opening channel and consequently entry Na+ at this site [12]. The action potential between two adjacent nodes of Ranvier as the membrane potential is around +35 millivolts [11]. During the myelinated internode, energies of sodium/potassium pumping system, the Na+ come back out of the axon and K^+ comes back into the axon for tuning the equilibrium of ions among the intracellular (Scheme 1).

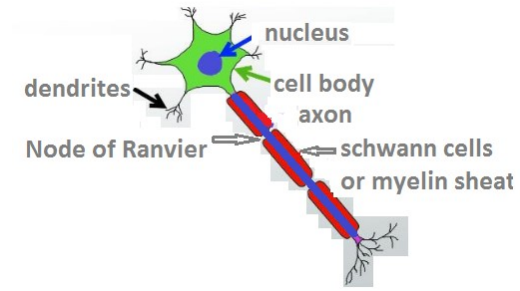

(A)

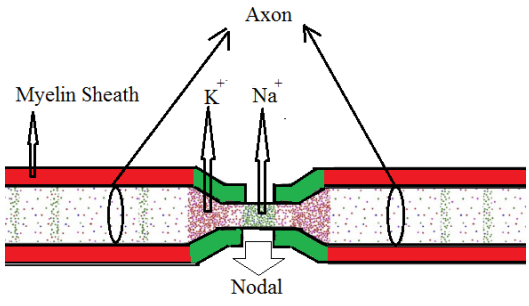

(B)

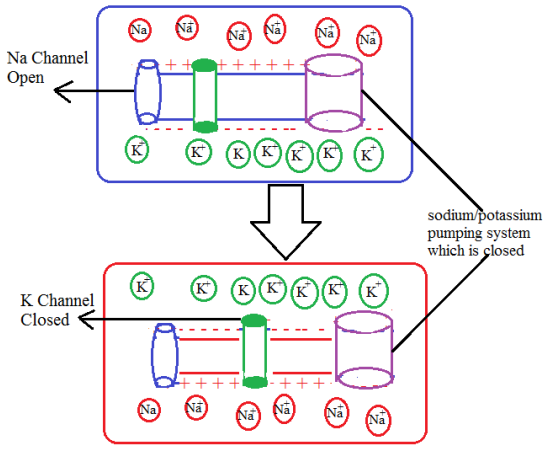

(C)

Scheme 1. (A) A part of Neuron; (B) schematic of sodium/potassium pumping System in the node of Ranvier (C) myelin-sheath.

The NOR includes the "Na+/K+ ATPases", "Na+/Ca2+" exchangers and great densities of voltages-gated Na+ channels which produce enough potential action for any electrical pulses. Sodium channel combined to alpha and beta subunits which anchor the channel to both intra and extra-cellular components. The extra-cellular region of beta subunits can be associated with itself and some other proteins such as "Contactin" which causes to increase the surface expression of Na+ channels. Various extracellular proteins are located at nodes of Ranvier, including Versican, Tenascin-R, Phosphacan, and Bral-1, as well as proteoglycan [13].

1.1. Theoretical background.

1.1.1. Electromechanical pulses.

Neurons transmit information by an electrical impulse which works as action potential and has a velocity between 1 and 100 m/s. Neurons receive the pulses from dendrites and propagate the pulses with axon and connect to other cells via synapses electrically or sometimes chemically, therefore there are various neurons in viewpoint of shapes, sizes, and electrochemical properties which generally contain a nucleus and organelles surrounded by membranes. The membranes are a combination of a lipid bilayer whose proteins are embedded inside glycolipids.

Axon membrane includes some kinds of proteins which selectively transfer sodium and potassium ions in a voltage-dependent type. In other words, this model indicates that nerve axon is an electrical circuit in which the proteins are resistors and the membrane is a capacitor. Ions flow through the membrane along the nerve axon due to the voltage changes with the channel proteins. Obviously, nerves represent thickness and length variations under the influence of the action potential [14, 15]. In addition, the action potential can be excited through the heat during the nerve pulses, or even a mechanical stimulus. Interestingly, the integrated exchange of heat is zero, indicating of adiabatic systems for action potential. Therefore, a nerve pulse can also be stimulated through local cooling which indicates that heat changes take place during the action potential [16]. Briefly, the mechanical and the heat effects exhibit that the nerve pulse is an adiabatic and also reversible phenomenon as same as the propagation of the mechanical waves.

This means the propagating nerve pulse is an electro-mechanical wave due to a breakdown of membrane resistance. This concept is an alternative interpretation of nerves pulses based on membrane thermodynamic including entropy, volume, pressure, and enthalpy changes. Consequently, the pulses can be moving the same as velocity of sound in the membrane. Hodgkin and coworkers [17] exhibited; action potential is not only a reduction of the membrane potential and overshooting action potential as a result of increased sodium permeability but also is important. They investigated a system of voltage-clamp circuit for facilitating quantitative measurement of ionic currents from squid axon. They also suggested that membranes through a selective mechanism can be permitting the transition of sodium or potassium in a suitable voltage [18].

In an ionic exchange, the net current could be separated into 1- fast inward current carried by Na^+ ions, and 2- slow activated outward current carried by K^+ ions[19] which are results from independent permeation mechanisms for sodium and potassium ions in the membrane. This approach is known as ionic hypothesis (Scheme 2) [20]. Various ion currents contribute to the voltage signal of a neuron in which 3 of them are major including sodium current, potassium current, leak current that consists (mostly chloride ions) that their flow is controlled via their respective voltage's channels in a membrane. The semipermeable membrane segregates the interior section from the exterior cell. The glycolipids membranes are simulated as insulators which act as same as capacitor with capacitance "C_{mem}" while each protein as a resistances has a specific conductance or Z_i (i indicates a particular channel and ion). As soon as a changing of voltage (V_{mem}), two kind currents might be produced, first a capacitive current charging the capacitor and second ohmic currents via the proteins resistances. And total current I_{mem} is the sum of these two currents.

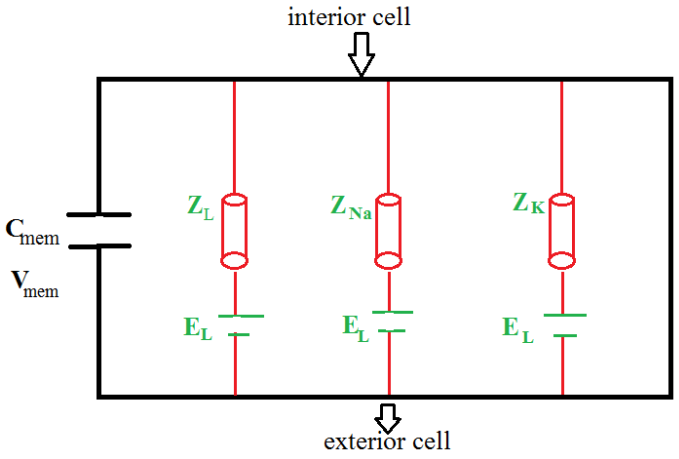

Scheme 2. A circuit of membranes including capacitor and ligands, sodium and potassium channels as resistance.

I_{mem} , is given by: $I_{mem}(t) = C_{mem}\frac{dV_{mem}}{dt} + Z_{Na}(V_{mem} - E_{Na}) + Z_K(V_{mem} - E_K) + Z_{Leak}(V_{mem} - E_{Leak})$ **(1)** where E_{Na}, E_K *and* E_{Leak} are the Nernst potentials of different ions. It also is given by equation $E_i = \frac{RT}{zF}Ln\frac{C_{out}}{C_{in}}$ where C_{out} and C_{in} are the concentrations of ions on the inner and outer side of the cell. This equation indicates that current flows due to diffusion along the gradients (even in the absence of other external voltages). Consequently, if the external voltage is equal to the Nernst potential, no current flows. Using Kirchhoff's laws, "cable theory" explains the investigating of a voltage along a cylindrical membrane as a function of distance x. The propagating action

potential can be estimated by: $\frac{\partial^2 V_{mem}}{\partial x^2} = \frac{2R_i}{\alpha} I_m$ where R_i is the specific inner resistance of the intracellular medium along the cable or through combining Eq. (1) with "cable theory", the equation (2) is given as follows [21,22]: $\frac{\partial^2 V_{mem}}{\partial x^2} = \frac{2R_{mem}}{\alpha}(C_{mem}\frac{dV_{mem}}{dt} + Z_{Na}(V_{mem} - E_{Na}) + Z_K(V_{mem} - E_K) + Z_{Leak}(V_{mem} - E_{Leak})$ **(2)** And R_{mem} is the specific resistance of the membrane. If it supposes the pulse propagates with a constant speed "θ" which is independent of voltage, consequently, the time dependent wave equation can be rewritten as: $\frac{\partial^2 V_{mem}}{\partial t^2} = \theta^2 \frac{\partial^2 V_{mem}}{\partial x^2}$ **(3)**. Combining Eq. (2) with Eq. (3) yields the propagation of the electrical pulse equation[23,24]: $\frac{\partial^2 V_{mem}}{\partial t^2} = \theta^2 \frac{2R_{mem}}{\alpha}(C_{mem}\frac{dV_{mem}}{dt} + Z_{Na}(V_{mem} - E_{Na}) + Z_K(V_{mem} - E_K) + Z_{Leak}(V_{mem} - E_{Leak})$ **(4).** for the mathematical treatment of action potential propagation along GalC of myelinated axons, we simulated a hybrid system of active elements coupled by passively conducting cables. Mathematical equation is described as; $C_{gal}\frac{\partial v}{\partial t} = \frac{1}{R_c}\frac{\partial^2 V}{\partial x^2} - \frac{V}{R_{gal}} + I_{chan}(v,t)$ **(5)**, here C_{gal} and R_{gal} are the (radial) capacitance and resistance of a myelinated fiber including Galactocerebroside, and R_c is its axial resistance. We choose these parameters in accordance with both experimental and simulation data. Although the currents generated via ion channels dynamics at the NOR are generally explained by a Hodgkin equations [17], there is a challenge for solving analytically for the mathematical mechanism.

2.2. Membrane contains Galactocerebroside (GalC) as a capacitor.

Galactocerebroside is lipid molecules which occur in large amounts in mammalian brain tissues, especially myelin. The primary lipid of myelin is a glycolipid called galactocerebroside which is a kind of cerebroside including of a ceramide with a galactose residue at the 1-hydroxyl section [25] (Fig.1). Pascher and coworkers [26, 27] through X-ray diffraction of cerebroside have shown that the structure of cerebroside bilayers have been generated through the galactose and sphingosine moieties in which the polar region of the bilayer including galactosyl aligned almost parallels to the bilayer interface. Several hydrogen bonds including donor and acceptor groups (CO, NH, OH) permit the formation of numerous lateral hydrogen bond systems between sphingosine and galactose in the amide moieties and the galactosyl, respectively. Additionally, anhydrous indicate evidence of complex polymorphic treatment and inter conversions between stable and metastable structural shapes. In some studies, the manner and stability of mixtures of human spleen glucocerebroside and mixtures of bovine brain cerebrosides and dipalmitoylphosphatidylcholine (DPPC) have been reported [28, 29].

Correa and coworkers [28] suggest that glucocerebroside distribution is affected via the physical state of the lipid bilayer and by the glucocerebroside/ DPPC molar ratio. Vibrational Raman spectra of the bovine brain kerosene mole fraction in mixtures with predict a disrupting of the cerebroside chain packing [30]. Although DPPC is a major constituent of myelin or other membranes, their mixture with GalC does permit a detailed structural analysis of their mutual interactions. Gal is presented in the myelin sheaths of Schwann cells in myelinating fibers of the ANS. GalC and sulfatide play major roles in the structure of Peripheral myelin. GalC and sulfatide are sphingolipids extremely enriched in myelin and the binding of reactive antibodies with either sulfatide or GalC to cultured oligodendrocytes causes a Ca^{2+} influx, followed by microtubule depolymerization. The cable equation of currents for potential propagation along GalC of myelinated axons yields a dynamics behavior. By this works, a small piece of cell membrane including pure GalC and DPPC with 50% mol ratio of each have been simulated for our model of membrane capacitors (Fig.2)

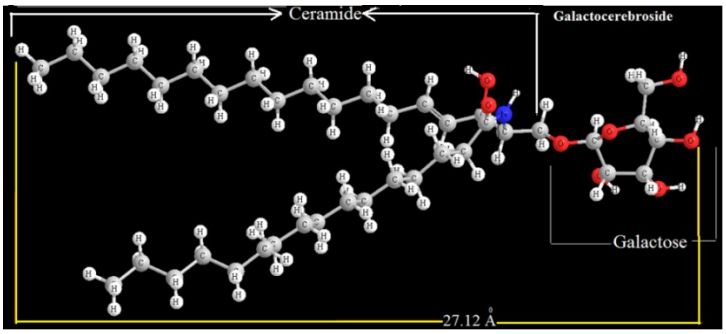

Figure 1. Optimized a molecule of Galactocerebroside (GalC) with cam-b3lyp/cc-pvdz basis set.

2.3. Membrane capacitor model.

During growth of a neuron, cell diameter can change considerably and neuronal elasticity may cause changes in the cell surface. Membrane electrical capacitance is a major cellular parameter for measuring cellular properties based on diameters or sizes changing. For instance, occasionally conductance densities for removing potential effect any changing in neuronal size to predict the proper mechanism has been calculated.

Various experimental ways exist to determine the total membrane surface that having a special membrane capacitance and are similar in most cells (commonly agreed with 0.5–1.0 F/cm^2) [31]. Capacitance can be calculated from the rate and amplitude changes in the voltage responses based on voltage clamp. These ways are applied widely to determine the total capacitance of several neurons membrane. By this work, we simulated our systems based on several membrane thicknesses in viewpoint of capacitors. In detail, Glial cell wraps around axons a few times (30-150 times) this like adding 330 membranes in the series. Therefore, through myelination the diameter of axon increases and speed of conduction increased by diameter of axon. In addition, potential action is related to $\frac{1}{r_a C_{membrane}}$ (scheme 3).

We compared the capacitance values of identified neurons cell membranes including GalC, DPPC and also a mixing of GalC/DPPC, (Fig.3). It has been shown that these mixed systems yield considerably differences values for the total membrane capacitance in the same circuits. These results yield suitable exponential voltages that are fitted by DC current in total membrane capacitance over vast ranges of cell sizes hav been simulated.

In an isovoltage cell, the results in a membrane potential change characterized by a single exponential (Eq. 6) with time constant $\tau_{mem} = r_{mem}C_{mem}$ where r_{mem} C_{mem} indicate the cell membrane resistance the total membrane capacitance, respectively. In such an isovoltage cell, r_{mem} is equal to the cell's input resistance R_{in} $V_{mem}(t) = V_{rest} + \sum_{i=0}^{\infty} V_i\,(1 - e^{-\frac{t}{\tau_i}})$ **(6),** the

maximum membrane potential change is given by $\Delta V_{mem} = V_{mem} - V_{rest} = R_{in}.I_{ext}$ **(7)** where I_{ext} is injected current phase. In a non-isovoltage cell, an equalizing process based on current flows among electrical compartments is accomplished [32].

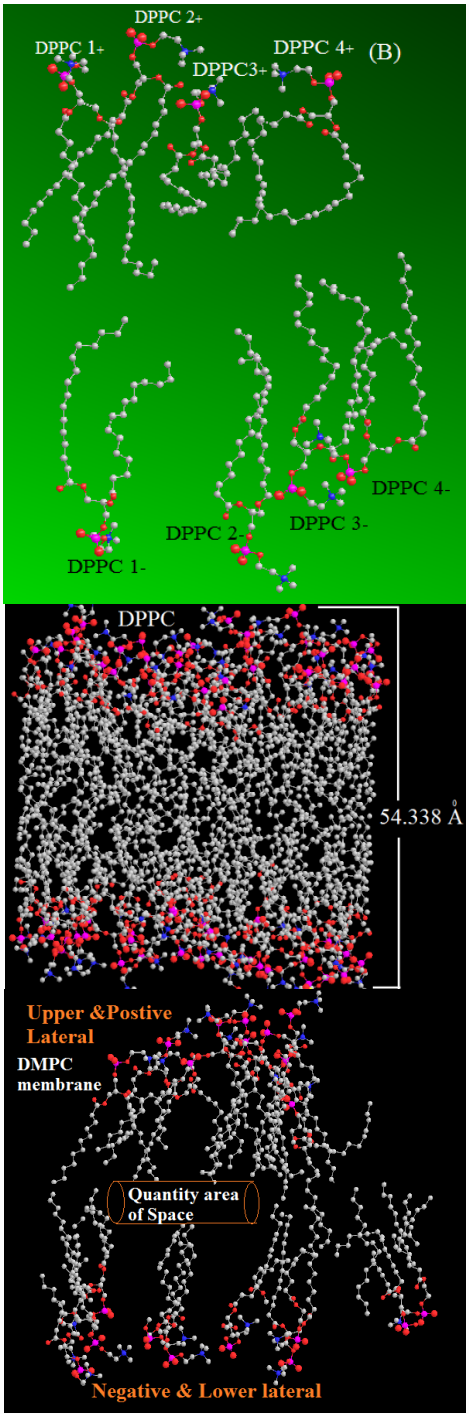

Figure 2. Monte Carlo calculation of DPPC membranes.

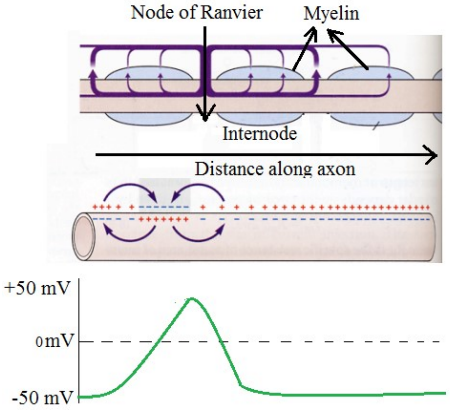

Scheme 3. Voltages changing of Myelin along axon.

Generally, only two or three terms adequately describe $V_{mem}(t)$, given by the equation (6) (Fig.4).

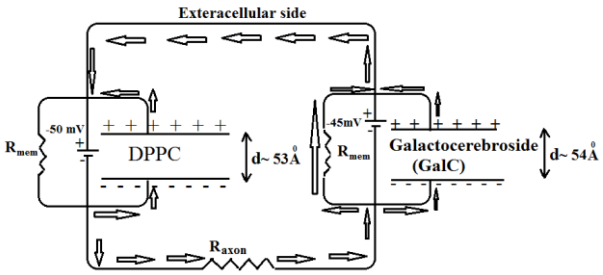

Figure 3. DPPC, GaLC in a circuit related to their thickness and their voltages.

Through dividing "I_{ext}" to a series of the resistive terms as $R_i = \frac{V_i}{I_{ext}}$ steady state can be evaluated as the sum of these resistive terms "$R_{in} = \frac{\Delta V_{mem}}{I_{ext}}$". The time constant of the slowest exponential ($e^{-t/\tau=0}$) corresponds to the membrane time constant $\tau_m = r_m C_m$ [34] . For determining the values of V_i and τ_i, the $V_{mem}(t)$ might be fitted with 2 or 3 exponential terms using the Levenberg–Marquardt (LM) algorithm. For obtaining the suitable fit in view point of both fast and slow components, the fitting has been done between t = 0 and a time at which the voltage had reached steady state (around 500-ms step). The capacitance, current and voltage of the membrane with total charge Q for related capacitor can be calculated by the following equations $Q = C_{mem}\Delta V_{mem} = \int_0^{t_{step}} I_c\, dt$. **(8)** Consequently, C_{mem} can be calculated according to $I_C = \frac{dQ}{dt} = C_{mem}\frac{dV_{mem}}{dt}$ **(9)** where $\frac{dV_{mem}}{dt}$ is slope of the voltage curve.

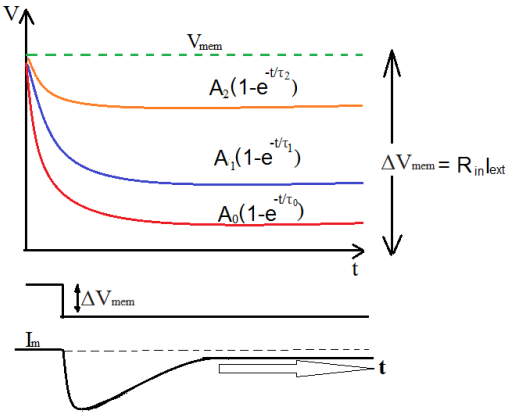

Figure 4. Schematic diagrams representing the membrane potential change, voltage-clamp step and the charge deposited on the membrane for a given"V_{mem}".

GalC/DPPC, Galc/ variable capacitance,$C_{mem}(t)$, defines the amount of charge (Q), which is stored on two electrodes at two sides of the membrane as a function of time $V_{mem}(t)$ Fig.3. Obviously, because of Nano scale characteristics in the cell membrane, quantum electrical properties might be taken into consideration. In a thin-membrane cell, this indicates that the geometric capacitance of the mentioned membranes, C_{mem}^{geo}, is related to the different voltages, "ΔV_{mem}" $C_{mem}^{geo} = \frac{\sigma}{\Delta V_{mem(t)}} = \frac{\varepsilon_r \varepsilon_0}{d_{mem(t)}}$ **(10).** Where "σ" is the surface charge density from total charges in two side of those membranes, "ε_0" is the permittivity from free spaces around "8.85 × 10^{-12} F.m^{-1} "and $d_{mem(t)}$ is the thickness expectation filling by the alkyl chain as a dielectric of the membranes. It is also a function of time due to dynamic behavior.

In this model, a tiny cell membrane capacitor is made by creating an insulating layer of alkyl between two galactose ("GalC") and phosphate of DPPC, groups. Supposing that each

capacitor plates carry $\pm Q$ charges from positive side to the negative side, the initial energies stored in an electrostatic field over the capacitor electrodes is given by $E_i = \frac{Q^2}{2C_{mem}}$. And for those systems that the charge $(Q + \Delta q_e)$ resides on the top plate and $(-Q - \Delta q_e)$ resides on the bottom plate, the accumulated energy is equal to "$E_f = \frac{(Q+\Delta q)^2}{2C}$". Although the charge is quantized by itself, the charges on both plates of the membrane capacitor are polarized. Obviously, the energy cannot be accumulated on the capacitors before a single electron tunnels through the alkyl layers from the (-) to the (+) sides, as: $\Delta E_s = E_f - E_i = \frac{\Delta q(Q+\frac{\Delta q}{2})}{C}$ **(11).** In this situation, the maximum voltage occurs in the range of $-\frac{\Delta q_{mem}}{2C_{mem}} < \Delta V_{mem} < +\frac{\Delta q_{mem}}{2C_{mem}}$ where the tunneling current would only flow if the voltage is sufficiently large, i.e. $|\Delta V_{mem}| > |\frac{q_{mem}}{2C_{mem}}|$. This effect is known as the Coulomb blockade [35].

Obviously, the expectation distances between two galactose lipids or phospholipids layers of the capacitor d_{mem} have to be extremely small such that the tunneling effect can take place with Acceptable sizes in the GalC/DPPC, membranes. In the macroscopic systems in the range of C~10^{-14} F, it can be shown that the voltages around $|\Delta V| > 1.4\mu V$ are needed for occurring the tunneling effect. For nano-scale capacitors with capacitances in the range of C ~ 10^{-17} F, the amount of $|\Delta V| > 1.4mV$ and for the nanoscale capacitor with the range of C~10^{-18} F, and the amount of $|V| > 0.70V$ are required for having a considerable tunneling effect. Thus, coulomb blockades cannot appear in macro-scaled circuits because of the low charging energies. However, it might occur in Nano-scales because of charge quantization [35]. For small items, the capacitances may be so trivial which the charging energy $\left(\frac{e^2}{2C_{mem}}\right)$ becomes larger and therefore the energies values for tunneling effect into the quantum system would then increase. The tunneling resistance can be estimated via $R_{Tun} = \frac{\Delta V_{mem}}{I_{mem}}$ which abnormal resistance is. However, it theoretically allows the electrons for crossing the insulating junctions as discrete occurrences which I_{mem} is the resulting currents because of tunneling effects. Tunneling resistances are not usual resistances, but an imaginary one, allowing the electrons for crossing the insulating junction during $t = R_{Tun}C_{mem}^{Qua}$ where C_{mem}^{Qua} is the quantum capacitance during tunneling events lifetime (t) of the energy state. TheR_{Tun}, might be finite and small, therefore the tunneling effect can practically occur. In this item, the charges are well quantized and so the capacitors are considered to be a tunnel junction in those mentioned membranes. In this work, R_{Tun} for those membranes as a function of thickness and potential energies barrier have been calculated: $\Delta E\, \Delta t \geq \frac{\hbar}{2} \rightarrow R_{Tun} \geq \frac{h}{2\pi q_e^2}$ **(12).** When the quantum well descends below the Fermi level, the electrons accommodate in the quantum well and the excess electrons in the membrane's phospholipids become sensitive for charging spilling. In these kinds of simulations, the expectation interlayer distances vary from 53.0 Å to 55.0Å (Fig.3) which is the best-optimized interaction in our model for various membranes. The hybrid quantum capacitances are related to a net capacitance,C_{mem}^{net}, and geometry capacitances C_{mem}^{geo} via equation as : $\frac{1}{C_{mem}^{net}} = \frac{1}{C_{mem}^{geo}} + \frac{2}{C_{mem}^{Qua}}$ **(13)** and the value of C_{mem}^{Qua} is in several orders of magnitude greater than the C_{mem}^{g}. Hence, its effect would only appear in quantum systems.

Based on the fluid mosaics model of lipids the dielectric constant for the above mentioned membrane change from time to time, while the changing in capacitances is not rapid. A quantum effect in the membrane implies that the capacitances of the membrane are larger than geometry of the membrane.

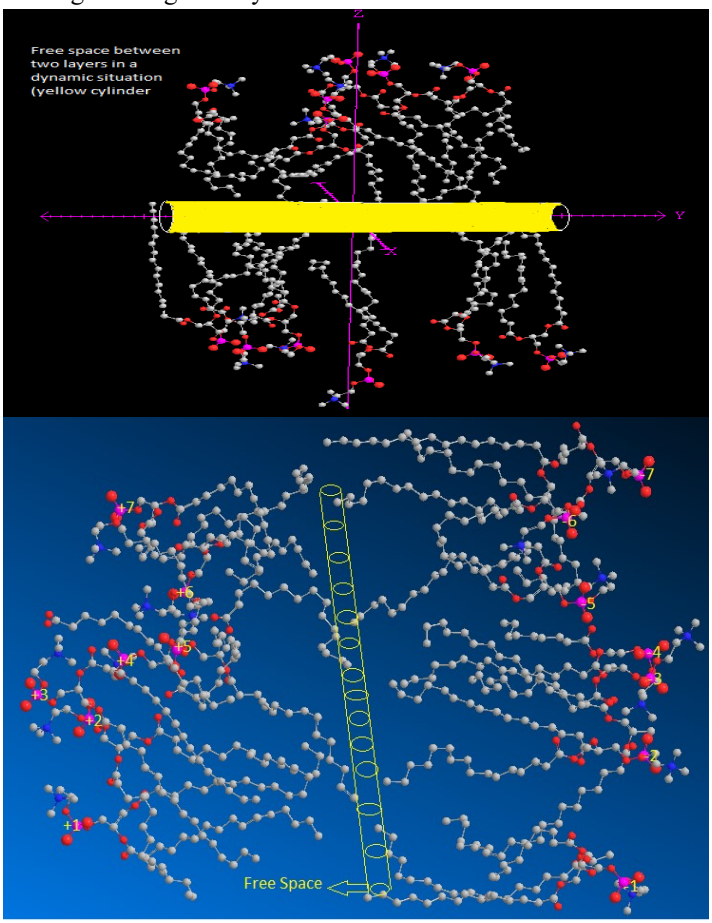

Figure 5. Free space between two layers in a dynamic situation due to tunneling coulomb blockade effect

Thus, any phenomenon in the bio-membrane related to the dynamic situation such as physiology temperature will influence their capacitances. It is also notable that the cellular electrical properties and electromagnetic fields on cells result in the electro biological mechanism and phenomena such as ligand receptor interactions in hormones, cell membrane activation and inhibition of cytoplasmic enzyme. Increasing the potentials and capacitances of those mentioned cell membranes alter the dipole orientation, activation of the DNA helix, increasing the codon transcription, increasing the codon translation in ribosome, and activating the cell membrane receptors that act as antennas for certain ranges of frequencies and amplitudes leading to the concepts of electromagnetic reception, transduction and attunement. It is also exhibited that the quantum effects are able to changing the membrane's capacitances due to the external effects. In addition, it is also concluded that the electrical properties of the membranes are affected via the application of electron densities in the above mentioned membranes. In our previous works, it has been declared [36- 65] that the quantum components are a manifestation of the density of states (Dos) of the phosphate or

galactose groups and their Thomas-Fermi screening lengths. Hence, the hybrid capacitance of any Nano-capacitor architecture is as follows:

$$C_{mem} = \left(\frac{1}{c_{mem}^{Qua}(one\ hand)} + \frac{1}{c_{mem}^{geo}} + \frac{1}{c_{mem}^{Qua}(opposite\ hand)}\right)^{-1} \quad \textbf{(14)}$$

where $c_{mem}^{Qua}(top\ side)$ and $c_{mem}^{qua}(down\ side)$ are the quantum capacitances due to the finite Dos of the phosphate group's electrodes, respectively, as illustrated in Fig.5.

A change in voltage leads to a capacitive current due to the changes in the charge on the capacitor which is given by: $\frac{dQ}{dt} = \frac{d}{dt}[(C_{mem}.V_{mem}] = C_{mem}\frac{dV_{mem}}{dt} + V_{mem}\frac{dC_{mem}}{dt}$ and

$$\frac{dC_{mem}}{dt} = f\left(\frac{dC_{mem}^{geo}}{dt}, \frac{dC_{mem}^{qua}}{dt}\right) \quad \textbf{(15)}$$

Heimburg exhibited that the changing voltages during the nerves pulses are completely dependent on the capacitances changing. In addition, transition voltages are able to exchange the ions. They have also exhibited how the electrical properties of the membranes are affected through the application of lateral pressure or tension in a membrane. By supposing that the C_{mem}^{geo} of bio-cell membranes (in contrast of C_{mem}^{qua}) is independent of voltage and depends on the geometry, the second term on the right side of eq.15 is a quantum effect ($\frac{dC_{mem}^{geo}}{dt} = 0$) [4].

Consequently, It can be considered that any changing in the dimension of the membrane through electrical phenomenon depends on C_{mem}^{qua} (and independent to C_{mem}^{geo}) which means tunneling effect changing due to the dynamic system in fluid mosaic model of membrane.

2. MATERIALS AND METHODS

Major Part of the membrane systems including GalC/DPPC, has been modeled with OMIOM (QM/MM) and Monte Carlo method. Each system contains 60 DPPC, and 120 GalC molecules (Figs 1&2). Each of systems, were accomplished with the lateral dimensions of the simulation cell $\{L_x\}$, consist of 53/54 for GalC/DPPC and 54/55 for Å while $\{L_y\}$ and $\{L_z\}$ are fixed with 50 and 100 Å, respectively for all components of the membranes. Three-dimensional periodic boundary situations were used, and the cell length normal to the various GalC/DPPC, membranes $\{L_z=100\}$ were allowed to adjust during the simulation to maintain a constant pressure around one atmosphere. These pressures were maintained through the variant of advanced systems formalism and also the Langevin Piston algorithm, which decreases oscillations in those cells parameters. The temperatures were fixed among 300K to 310K where are the biological ranges and identical to the relevant experiments. Configurations of individual lipids consistent with a mean field were generated by Monte Carlo (MC) simulation, with field values adjusted for obtaining acceptable with experimental order data. In this work, several force fields are applied with AMBER and Charmm software and in addition the Hyper-Chem professional release 7.01 programs are used for the drawing the graphs of simulation.

The final parameterization of GalC/DPPC, were computed using self-consistent field calculations in order for finding the optimal pre-geometries, as well as the total and partial charges of each side of membranes. DFT or density functional theories with the van der Waals interaction were applied to model the exchange-correlation energies of DPPC monomers. All optimization of monomer molecules of each membrane were performed through Gaussian 09. The main focus in this study is to obtain the results from DFT methods such as m062x, m06-L, and m06 for the (Myelin's lipids molecules)$_n$ {n=1-10}. The m062x, m06-L and m06-HF are advanced and novel functional with a suitable correspondence in non-bonded calculations between GalC/DPPC, and monomers and are useful for determining the voltages in viewpoint of distance differences distance between two lateral in two sides of Myelin's lipids. For non-covalent interactions between two layers of membranes, the B3LYP method is not suitable for describing van der Waals forces via medium-range interaction. Therefore, the QM/MM (ONIOM) methods including three sections of high (H), medium (M), and low (L) levels of calculations have been performed. For the first layer of ONIOM (QM/MM), DFT methods and for the second layer semi empirical pm6 (including pseudo=lanl2) and for the third layer Pm_3MM are applied for the high, medium and low sections, respectively. The semi empirical methods have been accomplished in order to the non-bonded interactions between two parts of the upper lateral side (P_+) and a lower lateral side (P_-) of Myelin's lipids. Some recent studies have exhibited an inaccuracy for the medium-range exchange energies leads to large systematic errors in the prediction of molecular properties. Geometries and electronic properties have been calculated using m06 (DFT) functional which is based on an iterative solution of the Kohn-Sham equation [66] in a plane-wave set and the Perdew-Burke-Ernzerhof (PBE) [67] exchange-correlation (XC) is also used. The charging transfers and electrostatic potentials were also estimated using the Merz-Kollman-Singh [68], chelp, or chelpG. These methods based on molecular electrostatic potential (MESP) fitting are not well-suited for evaluating larger systems due to the innermost atoms which are located far away from the center points. Therefore, the atomic charges for membranes must be computed as average data over several distances of membrane thickness. The interaction energies for membrane capacitors were measured as follows:

$$E_S(eV) = \{E_C - (\sum_{i=1}^{n}(Positive\ \text{Myelin's lipids})_i + \sum_{i=1}^{n}(Newgative\ \text{Myelin's lipids})_i)\} + E_{BSSE} \quad \textbf{(16)}$$

Where the "ΔE_S" is the stabilities energies of membrane capacitor. The electron densities, value of orbital wave-functions, electron spin densities, electrostatic potentials, electron localization functions (ELF), localized orbital locators (LOL) which defined by Becke & Tsirelson), total electrostatic potentials (ESP), as well as the Multifunctional Wave-function analyzing have been calculated with Multiwfn software [69]. The contour line map was also drawn using the Multiwfn software [69]. This is specifically useful to analyze distribution of electrostatic potential on VdW surfaces of each lateral side of Myelin's lipids. The relief maps were used to present the height value at every point of the capacitors. Shaded surface maps and shaded surface maps with projection are used in our representation of height value at each situation of voltages too [70]. In this work also, the interlayer attractions have been calculated through QM/MM with an ONIOM method including OPLS (CHARMM), force fields and Extended-Huckel for specific layers for describing their interlayer

interactions including inter-layer potentials, attractive components and the classical mono-polar electrostatic terms.

3. RESULTS

We used model descriptive structures of several membranes including GalC/DPPC, with the simplest consisting of two spheres attached to the related ends of a cable, which denote neuritis (l_{length} & $d_{diameter}$). We modeled variations in neuronal component size through changingl_{length} & $d_{diameter}$ (Table.1). In our model, the myelinated axon is a nearly circular profile surrounded by a spirally wound multi-lamellar sheath and has been wrapped with a medium number (n=100) of myelin sheath (Table.1).

Table 1. Geometries of Node Ranvier, Myelin and Myelin-sheath based on Monte Carlo and QM/MM calculation

membrane	d_{node} n = 10 (μm)	d_{myelin} n=100 (μm)	$d_{myelin-sheat}$ n=1 (Å)	l_{node} (μm)	l_{myeli} (μm)	C_{noda} $\mu F/cm^2$	C_{axon} $\mu F/cm^2$	Dielectric Constant K_{mem}
GalC/DPPC	0.10	0.55	54/53	0.65	1.75	2.0 *	0.55	6.29

* refer to reference 70 [70]

The expectation of dielectric thickness of GalC/DPPC, is 6.29 and 4.35 respectively for 60, 120 and 120 pieces of GalC/DPPC, of the membrane respectively (based on Gaussian's curve distribution) (Fig.6). The electron densities profiles, displayed in Figure 7, have been plotted from the electron densities profile models via dividing the simulation cells and determining the time-averaged number of electrons in each slab. The peaks exhibit the situation of the electron-rich Galactose/ Phosphate section of the head groups and the peak-to-peak distances are often used to derive the molecular length changing in length from the experimental data. Head groups area and the lateral diffusion coefficients for motion parallel for the membranes can be estimated. For construction a model of the membrane layers of lipids molecules, it is assumed which the CH_2 and terminal CH_3 groups presented in the hydrocarbons fatty acids chains fill the spaces in the center of the bilayer that is also symmetrical. The groups are considered for having same volumes as they occupy in the liquid hydrocarbons. The head groups form the layers of electron densities higher than that of water, while the fatty acid's chains from a layer with lower electron densities than that of water. The fatty acid's chains layers give negative amplitude which decreases rapidly if the layers are uniform and less rapidly if the terminal methyl groups are localized near the center, in order to give a narrow area of lower electron densities.

Table 2. Dielectric constant, capacitance and the stability energies of various modeled membrane capacitors in various thicknesses for GalC/DPPC capacitor.

GalC/DPPC & Number of atoms	$\Delta E_S(eV)$	$\Delta V = \Delta(\sum V_{P_+}^{1toN} \sum V_{P_-}^{1toN})$	$\Delta Q = \Delta(\sum Q_{P_+}^{1-N} - \lvert \sum Q_{P_-}^{1-N} \rvert)$	$C_g(F) \times 10^{20}$
(N=50)	0.0	-	-	-
(N=100)	+0.30	3.5	1.12	2.1
(N=200)	+1.25	3.2	1.42	4.7
(N=400)	0.95	4.9	1.63	1.2
(N=500)	+0.65	5.4	1.65	1.4
(N=600)	0.45	5.6	1.85	1.3
(N=3000)	1.45	5.75	1.90	1.3

In this work, GalC/DPPC, were chosen as the mixed membranes capacitors since the alkyls groups are an excellent space filling, similar to that of biological system. Since the alkyl chains in those membranes have an ideal electrical insulator that might be polarized through applying the external electrical fields, the expected thickness of alkyl's layers between those membranes plates have been estimated, optimized and applied as a excellent model of dielectric constant for those capacitances calculations (Table 2).

Same as other capacitors, the an-isotropic attachment of alkyl groups allows the formation of several layered structures. Long-ranges interlayers interactions play a prevailing role in characterizing the electrical and mechanical properties of those systems and hence their efficiency in these model of capacitors. The ESP curve is drawn versus the number of lipids in Fig.7 where the minimum values of the ESP correspond to the odd numbers of lipids. However, as for the even numbers, the ESP values are constant, indicating that the variable capacitances in those membranes are independent of number of lipids. This means, what makes the cell membranes for acting as a model of variable capacitors do not related to the internal structures, though; they depend on the external cellular effects the same as electrical situations and any other pulses. The interaction energy between two sides of membrane (P_{+30}, P_{-30}) of the electrodes) is also calculated based on (eq.16). The dielectric permittivity as a function of capacitor sizes was calculated using QM/MM methods (Table 2). The calculated values of the lipids structure such as distances between two layers, dielectric constants, (k), magnitude of the charges on each side of membranes, electrostatic properties using the SCF densities, fitting potential charges from ESP, stabilities energies of GalC/DPPC, as the capacitors, are listed in tables 2 & 3. The potential between two layers, $\Delta V = \Delta(\sum V_{P_+}^{1-N} - \sum V_{P_-}^{1-N})$ (a.u.) are listed in table 2 and vary between 3.5 and 5.75 volts for various thicknesses and number of lipids.

Table 3.The dielectric and capacitance C_Q= quantum capacitance, C_g= geometry capacitance, and C_{net}= net capacitance of modeled of GalC/DPPC capacitor in various thicknesses

GalC/DPPC & Number of atoms	$C_Q(F) \times 10^{19} = \frac{\Delta q(Q + \frac{\Delta q}{2})}{\Delta E_S}$		$C_{net}(F) \times 10^{19} = \frac{C_g C_Q}{C_Q + 2C_g}$
	ESP	Mulliken	ESP Mulliken
(N=500)	1.45	1.55	1.30 1.25
(N=600)	1.15	1.38	1.03 0.97
(N=2000)	1.66	1.83	1.17 1.20
(N=3000	1.43	1.56	0.99 0.99

The nano-capacitances of C_g , C_Q and C_{net} for GalC/DPPC, in different thickness of dielectrics are listed in table 3. Although the dielectric strength can be deduced from the band gap of alkyl space filler, the dielectric constant is directly calculated from eq. 5 which is much more accurate than the other ways. For large dielectric thicknesses, the classical capacitances of the "$C_g \propto \frac{1}{d}$" is conformable. This conformability is not valid for

short distances due to the quantum effect, therefore the dielectric permittivity as a function of dielectric size has been defined through, $C_Q(F) \times 10^{20} = \frac{\Delta q(Q+\frac{\Delta q}{2})}{\Delta E_S}$ *and* $C_{net}(F) \times 10^{20} = \frac{C_g C_Q}{C_Q + 2C_g}$. It is shown in this study that quantum effect has appeared in a small region of the membrane thickness due to number of lipid bi-layers.

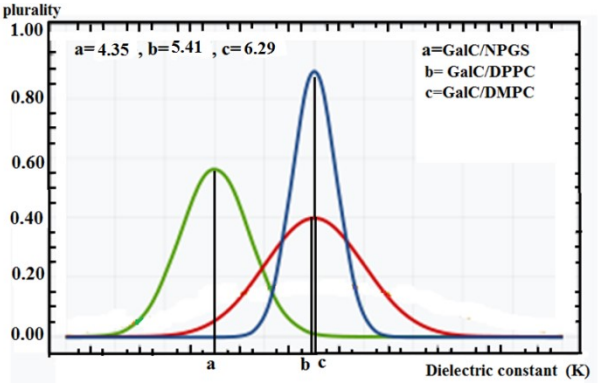

Figure 6. The expectation of dielectric constant for three systems of a, b and c Based on Gaussian curves

In the presence of any fields, Myelin's protein including trance membrane or potassium or sodium channel ions, charges employ the forces which can influence the position of the membrane in the Myelin; thereby influencing the variable fields makes variable capacitances in the membrane systems of GalC/DPPC.

This effect allows one to introduce a capacitive susceptibility that resonates with self-induction effect of helical coils in Myelin's proteins. Table.4 exhibits the calculated helical proteins self-induction of Myelin's proteins via resonance with capacitance of the GaLC/DPPC lipids or other Myelin membrane's lipids (Fig.8). Coils have greater inductance than straight conductors, thus, in biological phenomena, a helical coil of trance myelin's proteins resonate with a capacitive susceptibility of lipids capacitors of GalC/DPPC

Table 4. The self-induction of GaLC/DPPC modeled capacitors (N=300) with some Myelin's proteins.

Myelin proteins	Number of units	Resonance frequency
2WUT	1	65 GHZ
6IGO	3	55 GHZ
neuronal SNARE	2	45 GHZ

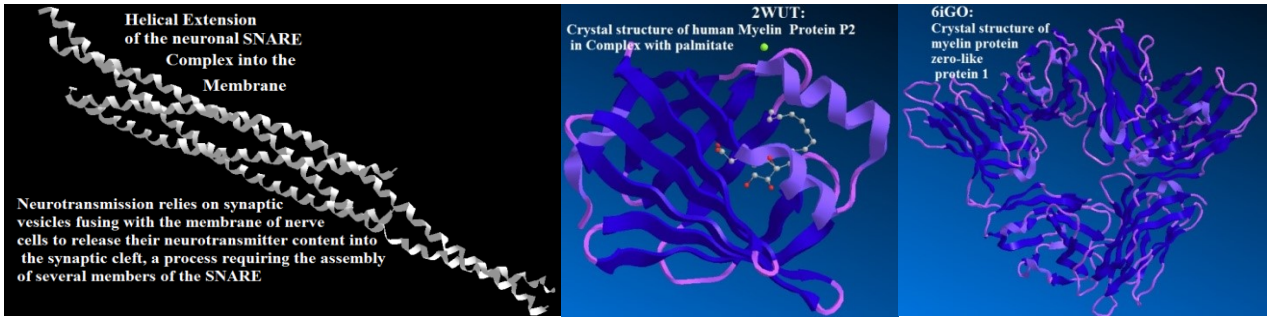

Figure 7. Myelin's Protein and Helical Extension of the neuronal SNARE complex into the Myelin membrane

4. CONCLUSIONS

When a protein is coiled, the magnetic field produced by current flow expands across adjacent coil rings. Since the current changes, the created induced magnetic field also changes. These changes create a force (emf) that opposes the changes in those currents. These effects do not occur in the static conditions in GalC/DPPC, myelin's membranes due to the steady currents. These impacts only appear and arise in the variable capacitors when the current experiences a changing in its value. When currents flow quickly, the magnetic field also collapses quickly and is capable to generate high induced electro motoric forces (emf) which at times can be several times the original amounts of the sources voltages. Higher induced voltages might be created in inductive circuits through increasing the rate of changes in the currents as well as increasing the number of coils in myelin's helical proteins. Myelin's membrane proteins as electrical inductors might enable the membrane cell to transiently produce very high electrical voltages such as Bio-Nano-Antenna.

5. REFERENCES

1. Keizer, J.; Smith, G.D.; Ponce-Dawson, S.; Pearson, J.E. Saltatory propagation of Ca2+ waves by Ca2+ sparks. *Biophysical Journal*. **1998**, *75*, 595–600, https://doi.org/10.1016/S0006-3495(98)77550-2.

2. Boullerne, A.I. The history of myelin. *Experimental Neurology*. **2016**, *283(Pt B)*, 431–45, https://dx.doi.org/10.1016%2Fj.expneurol.2016.06.005.

3. Salzer, J.L. Clustering sodium channels at the node of Ranvier: close encounters of the axon-glia kind. *Neuron*. **1997**, *18*, 843–846, https://doi.org/10.1016/S0896-6273(00)80323-2.

4. Monajjemi, M. Cell membrane causes the lipid bilayers to behave as variable capacitors: A resonance with self-induction of helical proteins. *Biophysical Chemistry* **2015**, *207*, 114-127, https://doi.org/10.1016/j.bpc.2015.10.003.

5. Swire, M.; Ffrench-Constant, C. Seeing Is Believing: Myelin Dynamics in the Adult CNS. *Neuron*. **2018**, *98,* 684–686, https://doi.org/10.1016/j.neuron.2018.05.005.

6. Hill, R.A.; Li, A.M.; Grutzendler, J. Lifelong cortical myelin plasticity and age-related degeneration in the live mammalian brain. *Nature Neuroscience* **2018,** *21,* 683–695, https://doi.org/10.1038/s41593-018-0120-6.

7. Hughes, E.G.; Orthmann-Murphy, J.L.; Langseth, A.J.; Bergles, D.E. Myelin remodeling through experience-dependent oligodendrogenesis in the adult somatosensory cortex.

Nature Neuroscience **2018**, *21*, 696–706, https://doi.org/10.1038/s41593-018-0121-5.
8. Hartline, D.K. What is myelin? *Neuron Glia Biology* **2008**, *4*, 153–63, https://doi.org/10.1017/S1740925X09990263.
9. Salzer, J.L.; Zalc, B. Myelination. *Current Biology* **2016**, *26*, R971–R975, https://doi.org/10.1016/j.cub.2016.07.074.
10. Steinman, L. Multiple sclerosis: a coordinated immunological attack against myelin in the central nervous system. *Cell*. **1996**, *85,* 299–302, https://doi.org/10.1016/S0092-8674(00)81107-1.
11. Greer, J.M.; Lees, M.B. Myelin proteolipid protein-the first 50 years. The International Journal of *Biochemistry & Cell Biology* **2002**, *34,* 211–5, https://doi.org/10.1016/S1357-2725(01)00136-4.
12. Raine, C.S. Characteristics of Neuroglia. In: *Basic Neurochemistry: Molecular, Cellular and Medical Aspects(6th ed.).* Siegel, G.J.; Agranoff, B.W.; Albers, R.W.; Fisher, S.K.; Uhler, M.D. (eds.).Philadelphia: Lippincott-Raven, 1999.
13. Kaplan, M.R.; Cho, M.H.; Ullian, E.M.; Isom, L.L.; Levinson, S.R.; Barres, B.A. Differential control of clustering of the sodium channels Na(v)1.2 and Na(v)1.6 at developing CNS nodes of Ranvier. *Neuron*. **2001**, *30,* 105–119, https://doi.org/10.1016/S0896-6273(01)00266-5.
14. Tasaki, I.; Kusano, K.; Byrne, M. Rapid mechanical and thermal changes in the garfish olfactory nerve associated with a propagated impulse. *Biophys. J*. **1989**, *55*, 1033–1040, https://dx.doi.org/10.1016%2FS0006-3495(89)82902-9.
15. Iwasa, K.; Tasaki, I.; Gibbons, R.C. Swelling of nerve fibers associated with action potentials. *Science* **1980**, *210*, 338–339, https://doi.org/10.1126/science.7423196.
16. Kobatake, Y.; Tasaki, I.; Watanabe, A. Phase transition in membrane with reference to nerve excitation. *Adv. Biophys*. **1971**, *208*, 1–31.
17. Hodgkin, A.L.; Katz, B. The effect of sodium ions on the electrical activity of the giant axon of the squid. *J. Physiol*. **1989**, *108,* 37–77, https://dx.doi.org/10.1113%2Fjphysiol.1949.sp004310.
18. Hodgkin, A.L.; Huxley, A.F. A quantitative description of membrane current and its application to conduction and excitation in nerve. *J. Physiol*. **1952**, *117*, 500–544, https://dx.doi.org/10.1113%2Fjphysiol.1952.sp004764.
19. Hodgkin, A.L.; Huxley, A.F. Currents carried by sodium and potassium ions through the membrane of the giant axon of Loligo. *J. Physiol.* **1952**, *116*, 449–472, https://dx.doi.org/10.1113%2Fjphysiol.1952.sp004717.
20. Haeusser, M. The Hodgkin-Huxley theory of the action potential. *Nat. Neurosci*. **2000**, *3*, 1165, https://doi.org/10.1038/81426.
21. FitzHugh, R. Impulses and physiological states in theoretical models of nerve membrane. *Biophys. J*. **1961**, *1*, 445–466, https://doi.org/10.1016/S0006-3495(61)86902-6.
22. Nagumo, J.; Arimoto, S.; Yoshizawa, S. An active pulse transmission line simulating nerve axon. *Proc. IRE* **1962**, *50*, 2061–2070.
23. Hindmarsh, J.L.; Rose, R.M. A model of neuronal bursting using three coupled first order differential equations. *Proc. R. Soc. Lond. B* **1984**, *221,* 87–102, https://doi.org/10.1098/rspb.1984.0024.
24. Rajagopal, K. A generalized-model for the nerve impulse propagation. *Phys. Lett. A* **1983**, *99*, 261–264, https://doi.org/10.1016/0375-9601(83)90923-4.
25. Bologa-Sandru, L.; Zalc, B.; Herschkowitz, N.; Baumann, N. Oligodendrocytes of jimpy mouse express galactosylceram-100. *Biophysical Journal* **1981,** *43*, 1983.
26. Pascher, I.; Sundell, S. Molecular arrangements in sphingolipids. The crystal structure of cerebroside. *Chem. Phys. Lipids* **1977**, *20*, 175-191, https://doi.org/10.1016/0009-3084(77)90033-0.
27. Abrahamsson, S.; Pascher, I.; Larsson, K.; Karlsson, K.A. Molcular arrangements in glycolipids. *Chem. Phys. Lipids* **1972**, *8*, 152-179, https://doi.org/10.1007/978-1-4684-8127-3_1.
28. Correa-Freire, M.C.; Freire, E.; Barenholz, Y.; Biltonen, R.L.; Thompson, T.E. Thermo tropic behavior of glucose rebroside di palmitoyl phosphatidylcholine multilamellar liposomes. *Biochemistry* **1979**, *18,* 442-445, https://doi.org/10.1021/bi00570a008.
29. Linington, C.; Rumsby, M.G. Galactosyl ceramides of the myelin sheath: thermal studies. *Neurochem. Int.* **1981**, *3*, 211-218, https://doi.org/10.1016/0197-0186(81)90003-6.
30. Bunow, M.R.; Levin, I.W. Molecular conformations of cerebrosides in bilayers determined by Raman spectroscopy. *Biophys. J*. **1981**, *32*, 1007-1021, https://doi.org/10.1016/S0006-3495(80)85032-6,
31. Koch, C. *Biophysics of Computation: Information Processing in Single Neurons*. New York: Oxford Univ. Press. 1999.
32. Major, G.; Evans, J.D.; Jack, J.J. Solutions for transients in arbitrarily branching cables: I. Voltage recording with a somatic shunt. *Biophys J* **1993,** *65*, 423–449, https://dx.doi.org/10.1016%2FS0006-3495(93)81037-3.
33. Major, G.; Evans, J.D.; Jack, J.J. Solutions for transients in arbitrarily branching cables: II. Voltage clamp theory. *Biophys J* **1993**, *65*, 450–468, https://doi.org/10.1016/S0006-3495(93)81038-5.
34. Holmes, W.R.; Segev, I.; Rall, W. Interpretation of time constant and electronic length estimates in multi cylinder or branched neuronal structures. *J Neurophysiol* **1992**, *68*, 1401–1420, https://doi.org/10.1152/jn.1992.68.4.1401.
35. Klein, D.L.; Roth, R.; Lim, A.K.L.; Alivisatos, A.P.; McEuen, P.L. A single-electron transistor made from a cadmium selenide nanocrystal. *Nature (London)* **1997**, *389*, 699.
36. Mollaamin, F.; Monajjemi, M. DFT outlook of solvent effect on function of nano bioorganic drugs. *Physics and Chemistry of Liquids* **2012**, *50*, 596-604, https://doi.org/10.1080/00319104.2011.646444.
37. Mollaamin, F.; Gharibe, S.; Monajjemi, M. Synthesis of various nano and micro ZnSe morphologies by using hydrothermal method. *International Journal of Physical Sciences* **2011**, *6*, 1496-1500.
38. Ardalan, T.; Ardalan, P.; Monajjemi, M. Nano theoretical study of a C 16 cluster as a novel material for vitamin C carrier. *Fullerenes Nanotubes and Carbon Nanostructures* **2014**, *22,* 687-708, https://doi.org/10.1080/1536383X.2012.717561.
39. Mahdavian, L.; Monajjemi, M.; Mangkorntong, N. Sensor response to alcohol and chemical mechanism of carbon nanotube gas sensors. *Fullerenes Nanotubes and Carbon Nanostructures* **2009**, *17*, 484-495, https://doi.org/10.1080/15363830903130044.
40. Monajjemi, M.; Najafpour, J. Charge density discrepancy between NBO and QTAIM in single-wall armchair carbon nanotubes. *Fullerenes Nanotubes and Carbon Nano structures* **2014**, *22,* 575-594, https://doi.org/10.1080/1536383X.2012.702161.
41. Monajjemi, M.; Hosseini, M.S. Non bonded interaction of B16 N16 nano ring with copper cations in point of crystal fields. *Journal of Computational and Theoretical Nanoscience* **2013**, *10*, 2473- 2477.
42. Monajjemi, M.; Mahdavian L., Mollaamin F. 2008. Characterization of nanocrystalline silicon germanium film and nanotube in adsorption gas by Monte Carlo and Langevin dynamic simulation. *Bulletin of the Chemical Society of Ethiopia* **2008**, *22*, 277-286, http://dx.doi.org/10.4314/bcse.v22i2.61299.

43. Lee, V.S.; Nimmanpipug, P.; Mollaamin, F.; Thanasanvorakun, S.; Monajjemi, M. Investigation of single wall carbon nanotubes electrical properties and normal mode analysis: Dielectric effects. *Russian Journal of Physical Chemistry A* **2009**, *83*, 2288-2296, https://doi.org/10.1134/S0036024409130184.
44. Mollaamin, F.; Najafpour, J.; Ghadami, S.; Akrami, M.S.; Monajjemi, M. The electromagnetic feature of B N H (x = 0, 4, 8, 12, 16, and 20) nano rings:Quantum theory of atoms in molecules/NMR approach. *Journal of Computational and Theoretical Nanoscience* **2014**, *11*, 1290-1298.
45. Monajjemi, M.; Mahdavian, L.; Mollaamin, F.; Honarparvar, B. Thermodynamic investigation of enolketo tautomerism for alcohol sensors based on carbon nanotubes as chemical sensors. *Fullerenes Nanotubes and Carbon Nanostructures* **2010**, *18*, 45-55, https://doi.org/10.1080/15363830903291564.
46. Monajjemi, M.; Ghiasi, R.; Seyed, S.M.A. Metal-stabilized rare tautomers: N4 metalated cytosine (M = Li , Na , K, Rb and Cs), theoretical views. *Applied Organometallic Chemistry* **2003**, *17*, 635-640, https://doi.org/10.1002/aoc.469.
47. Ilkhani, A.R.; Monajjemi, M. The pseudo Jahn-Teller effect of puckering in pentatomic unsaturated rings C AE , A=N, P, As, E= H, F, Cl. *Computational and Theoretical Chemistry* **2015**, *1074*, 19-25.
48. Monajjemi, M. Non-covalent attraction of B N and repulsion of B N in the B N ring: a quantum rotatory due to an external field. *Theoretical Chemistry Accounts* **2015**, *134*, 1-22, https://doi.org/10.1007/s00214-015-1668-9.
49. Monajjemi, M.; Naderi, F.; Mollaamin, F.; Khaleghian, M. Drug design outlook by calculation of second virial coefficient as a nano study. *Journal of the Mexican Chemical Society* **2012**, *56,* 207-211.
50. Monajjemi, M.; Bagheri, S.; Moosavi, M.S. Symmetry breaking of B2N(-,0,+): An aspect of the electric potential and atomic charges. *Molecules* **2015**, *20,* 21636-21657, https://doi.org/10.3390/molecules201219769.
51. Monajjemi, M.; Mohammadian, N.T. S-NICS: An aromaticity criterion for nano molecules. *Journal of Computational and Theoretical Nanoscience* **2015**, *12*, 4895-4914, https://doi.org/10.1166/jctn.2015.4458.
52. Monajjemi, M.; Ketabi, S.; Hashemian, Z.M.; Amiri, A. Simulation of DNA bases in water: Comparison of the Monte Carlo algorithm with molecular mechanics force fields. *Biochemistry (Moscow)* **2006**, *71*, 1-8, https://doi.org/10.1134/s0006297906130013.
53. Monajjemi, M.; Lee, V.S.; Khaleghian, M.; Honarparvar, B.; Mollaamin, F. Theoretical Description of Electromagnetic Nonbonded Interactions of Radical, Cationic, and Anionic NH2BHNBHNH2 Inside of the B18N18 Nanoring. *J. Phys. Chem C* **2010**, *114*, 15315, http://dx.doi.org/10.1021/jp104274z.
54. Monajjemi, M.; Boggs, J.E. A New Generation of BnNn Rings as a Supplement to Boron Nitride Tubes and Cages. *J. Phys. Chem. A* **2013**, *117,* 1670-1684, http://dx.doi.org/10.1021/jp312073q.
55.Monajjemi, M. Non bonded interaction between BnNn (stator) and BN B (rotor) systems: A quantum rotation in IR region. *Chemical Physics* **2013**, *425*, 29-45, https://doi.org/10.1016/j.chemphys.2013.07.014.
56. Monajjemi, M.; Robert, W.J.; Boggs, J.E. NMR contour maps as a new parameter of carboxyl's OH groups in amino acids recognition: A reason of tRNA–amino acid conjugation. *Chemical Physics* **2014**, *433*, 1-11, https://doi.org/10.1016/j.chemphys.2014.01.017.
57. Monajjemi, M. Quantum investigation of non-bonded interaction between the B15N15 ring and BH2NBH2 (radical, cation, and anion) systems: a nano molecularmotor. *Struct Chem* **2012**, *23*, 551–580, http://dx.doi.org/10.1007/s11224-011-9895.
58. Monajjemi, M. Metal-doped graphene layers composed with boron nitride–graphene as an insulator: a nano-capacitor. *Journal of Molecular Modeling* **2014,** *20*, 2507, https://doi.org/10.1007/s00894-014-2507-y.
59. Monajjemi, M. Graphene/(h-BN)*n*/X-doped raphene as anode material in lithium ion batteries (X = Li, Be, B AND N). *Macedonian Journal of Chemistry and Chemical Engineering* **2017**, *36,* 101–118, http://dx.doi.org/10.20450/mjcce.2017.1134.
60. Monajjemi, M. Study of CD5+ Ions and Deuterated Variants (CHxD(5-x)+): An Artefactual Rotation. *Russian Journal of Physical Chemistry a* **2018**, *92*, 2215-2226.
61. Monajjemi, M. Liquid-phase exfoliation (LPE) of graphite towards graphene: An ab initio study. *Journal of Molecular Liquids* **2017**, *230*, 461–472, https://doi.org/10.1016/j.molliq.2017.01.044.
62. Jalilian, H.; Monajjemi, M. Capacitor simulation including of X-doped graphene (X = Li, Be, B) as two electrodes and (h-BN)m (m = 1–4) as the insulator. *Japanese Journal of Applied Physics* **2015**, *54*, 085101-7
63. Phm, T.T.; Monajjemi, M.; Dang, C. M., Fabrication of lithium-ion batteries based on various LiNi1–*x*Co*x*O2 cathode materials. *Int. J. Nanotechnol.* **2018**, *15*, 925-935, https://doi.org/10.1504/IJNT.2018.099932.
64. Monajjemi, M.; Dang, C.M.; Alihosseini, A.; Mollaamin, F. Designing BN sheets of X-G//(h-BN)n//X-G (X = B, N) and GO/h-BN/GO structures for based anodes material to improve the performance of lithium-ion batteries. *Int. J. Nanotechnology* **2018**, *15*, 819-844, https://dx.doi.org/10.1504/IJNT.2018.099925.
65. Thi, L.C.M.; Blanc, E.F.; Monajjemi, M.; Dang, C.M. Theoretical and experimental simulation of inkjet printing process: investigation of physical parameters of a droplet. *Int. J. Nanotechnol* **2018**, *15,* 845-857, https://doi.org/10.1504/IJNT.2018.099926.
66. Kohn, W.; Sham, L.J. Self-Consistent Equations Including Exchange and Correlation Effects. *Phys. Rev A* **1965**, *140,* 1133-1138, https://doi.org/10.1103/PhysRev.140.A1133.
67. Perdew, J.P.; Burke, K. Generalized Gradient Approximation Made Simple. *Phys. Rev. Lett* **1996**, *77*, 3865-3868, https://doi.org/10.1103/PhysRevLett.77.3865.
68. Besler, B.H.; Merz, K.M.; Kollman P.A. Atomic charges derived from semiempirical methods. *Comp. Chem* **1990**, *11*, 431-439, https://doi.org/10.1002/jcc.540110404
69. Lu, T.; Chen, F. Multiwfn: A Multifunctional Wavefunction Analyzer. *J. Comp. Chem.* **2012**, *33,* 580-592, https://doi.org/10.1002/jcc.22885.
70. Frankenhaeuser, B.; Huxley, A.F. The action potential in the myelinated nerve fiber of Xenopus laevis, as computed on the basis of voltage clamp data. *J. Physiol.* **1964**, *171*, 302–315, https://dx.doi.org/10.1113%2Fjphysiol.1964.sp007378.